TUDelft

Delft University of Technology

Experimental broadband signal reconstruction for plate-like structures

Venturini, Nicolas; Martinez, Marcias; Troiani, Enrico; Barroso-Romero, Maria; Falcetelli, Francesco

Important note
To cite this publication, please use the final published version (if applicable).
Please check the document version above.

Experimental Broadband Signal Reconstruction for Plate-like Structures

Nicolas Venturini[1,2]*, Marcias Martinez[1]*,[3], Enrico Troiani[2]*, Maria Barroso-Romero[3],
Francesco Falcetelli[2]*

[1] Clarkson University, Department of Mechanical and Aeronautical Engineering, Potsdam, NY, 13699, USA.
*mmartine@clarkson.edu

[2] University of Bologna, Department of Industrial Engineering, via Zamboni 33, 40126, Bologna, Italy.
*nicolas.venturini@studio.unibo.it

[3]Faculty of Aerospace Engineering, Delft University of Technology, Kluyverweg 1, 2629 HS Delft,
Netherlands
*M.BarrosoRomero@tudelft.nl

Abstract

In the Structural Health Monitoring (SHM) field, the Acoustic Emission (AE) technique is a passive method by which damage is localized and identified by capturing Lamb Waves (LW) signals propagating in a plate-like structure. The reconstruction of emitted signals from damage at the source location constitutes one of the main challenges faced by the SHM community. Recently, the application of a Frequencies Compensation Transfer Function (FCTF) has been used to reconstruct narrowband (NwB) and broadband (BdB) signals through a hybrid experimental and numerical Time Reversal (TR) process on aluminum plates. This study aims to reconstruct through experimental methods different types of NwB and BdB signals on different plate-like structures making use of FCTFs. In particular, Hanning Window (HW) and Numerical Band Limited Broadband (NBLB) signals have been reconstructed for aluminum and steel plates. The results obtained in this study show how the FCTF method can be applied to different types of materials in plate-like structures. Moreover, the FCTF method has been applied on real BdB signals emitted by the Pencil Lead Break (PLB) technique and Rock Impact (RI) test. These last results prove that the FCTF method is able to compensate for the frequency changes on a single wave packet. Such results are fundamental, as they open the possibility to reconstruct any type of source signals emitted by any damage type.

1. Introduction

The Acoustic Emission (AE) method is one of the Structural Health Monitoring (SHM) techniques used for damage localization in critical assets. SHM can be defined as the process of implementing an in-situ real time damage localization, quantification and identification strategy for critical structures [1]. In particular, AE is the process by which acoustic signals are generated through the formation of a damage on a structure. Successively, the acoustic signal is captured by sensors, analyzed and used to determine the location of the damage over the monitored structure through a localization algorithm. As such, the AE method can be categorized as a passive method in the SHM field [2] since the sensors are only used to ''listen'' to the propagation of acoustic emissions on the structure. Different types of damage can produce the source of an AE event. For isotropic plate-like structures, a crack propagation can be the source of AE events [3], whereas for anisotropic structures, such as composite material structures, a delamination or a fiber breakage can cause the generation of an acoustic emission event [4]. In addition, other types of material degradation events can lead to the emission of an AE signal such as for example impacts [5], yielding [6], fretting [7] and friction [8]. However, one of the primary challenges faced by the SHM community is attempting to model these AE signals. Thus, the need to determine if the application of the Time Reversal (TR) method in combination with a system transfer function can be used for obtaining the original signal of an AE event.

In the case of a plate-like structure, a damage generates a specific type of elastic waves called Lamb Waves (LW), as discovered by Horace Lamb in 1917 [9]. The Lamb Waves are mathematically described by the set of *Rayleigh-Lamb Equations*. This set contains two equations representative of the propagation modes of the LW in a plate. Such modes are the symmetric modes, denoted by S_i, and the anti-symmetric modes, denoted by A_i. Often, the damage localization strategies in plate-like structures available in the literature are based on the measurement of the Time of Arrival (ToA) of the LW modes as an input to a triangulation localization algorithm, as the modes propagate at different speeds.

In order to calibrate localization algorithms in a laboratory setting, researchers make use of different active methods, developed over the years. These methods aim to induce LW signal in a plate-like structure. Actuators and sensors in AE systems are commonly made from Lead Zirconate Titanate (PZT) discs surface-bonded or embedded. PZT sensors are known to convert mechanical deformation from the passing of an elastic wave into an electrical signal and vice-versa, that is to say that electrical signals will generate a mechanical deformation when the PZT discs act as an actuator. A common test signal produced using PZT actuators for calibration of AE systems is the Hanning Window (HW), first introduced by J.F. Von Hann in 1903 [10]. The HW signal finds its specificity in the frequency domain since its Fast Fourier Transform (FFT) contains one central frequency peak. The signals with such property are commonly called narrowband signals (NwB). However, the LW signals generated by a damage during operational-service conditions are broadband (BdB) in nature. A BdB signal is characterized by a FFT containing a multitude of peaks in the frequency domain. Thus, Hsu and Nielsen introduced the Pencil Lead Break (PLB) technique in 1981. Through the application of the PLB technique, a BdB signal is emitted simulating an AE source [11] by the breaking of a pencil lead on the surface of the structure. The use of a controlled impact has also been used for the generation of AE BdB signals [5].

The reconstruction of such BdB test signals in a computational modelling environment constitutes a challenge in the SHM field. There is a requirement to understand the original source of these AE events in order to implement new damage identification strategies. The first results on signal reconstruction were documented by M. Fink in 1992 through the use of ultrasonic waves, applying a Time Reversal (TR) technique to acoustic impulses in a pressure field [12]. This technique was also known as the Time Reversal Mirror (TRM) since at the end of the process, the received signal source is a time-reversed image of the input test signal. This methodology was then implemented for the reconstruction of acoustic waves and LW [13,14]. In 2003, CH. Wang et al. reconstructed Gaussian pulses between two PZT transducers [15] making use of the frequency dependent time reversal operator introduced by the Mindlin Theory [16]. Then, in 2007, V. Giurgiutiu and B. Xu reconstructed HW [17] thanks to the single mode and two modes tuning effects of PZT transducers [18]. H.W. Park et al. gave a theoretical interpretation to the presence of side bands observed during the reconstruction of HW in a two modes tuning modality in 2009 [19].

F. Falcetelli et al. introduced the idea of BdB signals reconstruction in 2018 [20] through a Frequencies Compensation Transfer Function (FCTF) using a hybrid experimental and numerical approach in order to reconstruct a PLB signal in an aluminum plate. Such hybrid FCTF method has been used once again in July 2019 by J. Wang and Y. Shen to reconstruct HW signals in an aluminum plate [21]. Furthermore, they demonstrated experimentally the reliability of the FCTF method for the HW reconstruction in aluminum. Nevertheless, the last works on the LW signal reconstruction through the FCTF did not show if this method can be extended to different types of materials [20,21]. Moreover, the BdB signal reconstruction on aluminum plate has never been demonstrated through an experimental approach. This study addresses as primary objective the reconstruction of NwB signal such as HW and Numerical Band Limited Broadband (NBLB) signals created on Matlab[TM] for an aluminum and a steel plate through the application of a FCTF. The secondary objective consists on the reconstruction of real BdB signals such as the ones emitted by a PLB and a Rock Impact (RI) in an aluminum plate. This last objective is important since it can open the perspective to reconstruct any type of signal emitted by any type of damage through the hybrid approaches presented in [20,21].

2. Methodology

The methodology for the experimental reconstruction of signals follows a precise path which is divided in several sub-sections:

2.1. *Signal Sources***:** Different types of source signal are used as input at PZT 1, as represented in Figure 1.a.

2.2. *Signal Reception:* Each source signal emitted at the source location propagates in the medium and is captured by a PZT transducer bonded to the structure (PZT 2).

2.3. *Plates***:** The PZT transducers are used for different plate structures (aluminum and steel plates). Figure 1 gives an example of the aluminum plate.

2.4. *Sensor Networks:* The sensor networks and the PZT transducers type are introduced for each plate. Figure 1 introduces the example of two Piezokinetics PZT transducers, PZT 1 and PZT 2, placed on the midline of the aluminum plate.

2.5. *Frequencies Compensation Transfer Function Creation Process:* The FCTF is built (Figure 1.c) thanks to a TR process of a Band Limited White Noise (BLWN) signal.

2.6. *Signal Reconstruction and Verification Process:* The signal reconstruction and verification process is performed. The TR process applied to the distorted version of the signal source presented in Figure 1.b and the successive application of the FCTF to the time-reversed output signal of the TR process allows for the reconstruction of the input signal as shown in Figure 1.d. Finally, the original input source signal and the reconstructed signal are exploited in different ways in order to implement different verification processes (Figure 1.e).
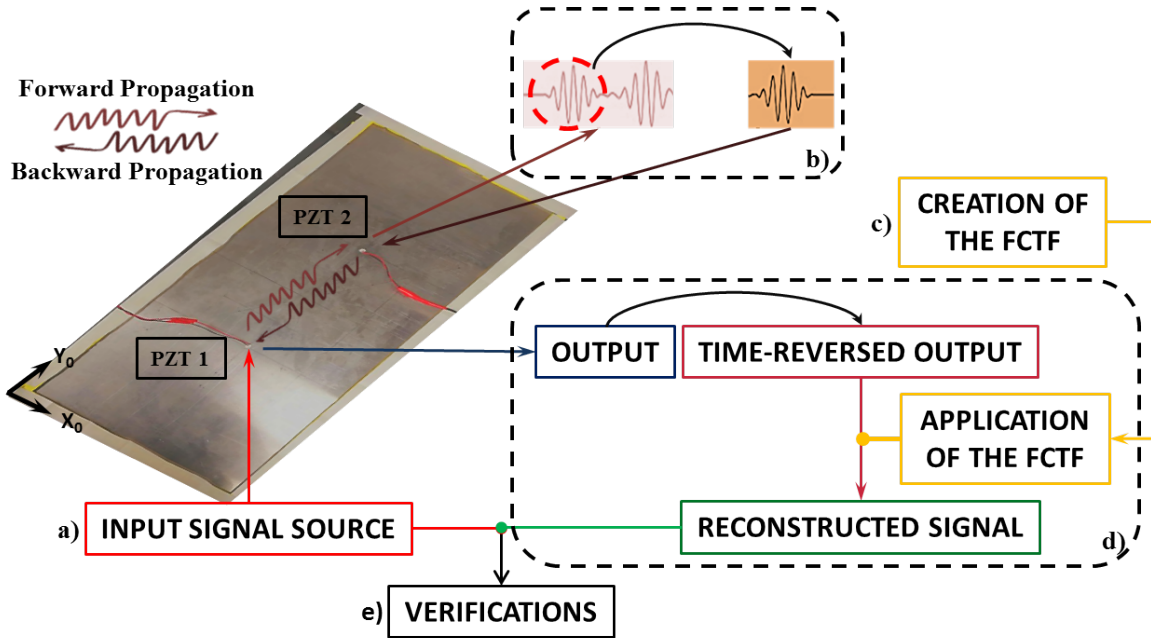

Figure 1: Overall methodology

2.1. Signal Sources

The AE signals can be divided in two families: the NwB signals and the BdB signals. One NwB signal and three BdB signals have been chosen for this study. The NwB signal consists of a HW with a central frequency at 350 kHz. The first BdB signal consists of a NBLB signal of 30 μs in a frequency range below 1 MHz. The two signals were produced in Matlab^{TM} and their amplitudes were mapped in the interval [-1,1]. In particular, the HW signal was created by applying equation (1) to a carrier sine wave with a frequency content of 350 kHz whereas the NBLB signal was designed thanks to random generator command in Matlab^{TM}. In equation (1), $T_H = N_B/f$, where N_B and f are the number of counts and the tone burst frequency of the HW respectively. The set-up, composed by the waveform generator Picoscope 3204-DMSO, the Broadband Power Amplifier ENI 240L and a PZT actuator fixed on a plate-like structure, allows for the amplification and emission of the signals so designed. This set-up is introduced in Figure 2.a.

$$H(t) = \frac{1}{2}\left[1 - \cos\left(\frac{2\pi t}{T_H}\right)\right] \qquad (1)$$

The second BdB signal was the PLB signal. Such signal was generated breaking the graphite lead of the Rotring Tikky Pencil following specific modalities as described in the American Standard ASTM E-976 [22]. Figure 2.b shows the application of the PLB technique following the ASTM E-976 standard.

The last BdB signal consisted on the signal emitted by a RI test. Small copper coated steel balls with a diameter and a weight of approximately 4.5 mm and 0.4 g respectively, are dropped from a specific height thus generating a BdB signal when the steel ball impacts the surface of the plate. In order to emit a repeatable and consistent signal from a desired location, the ball was guided through a funnel connected to a small diameter pipe. This particular set-up allows obtaining always the same starting height of approximatively 25 cm with respect to the plate. The RI test set-up is represented in Figure 2.c.

It is important to note that when HW and NBLB signals are used as input source signals, the emission is known a priori as these were designed by the authors in Matlab^{TM}. Nevertheless, if the PLB or RI techniques are used as source signals, the signal emitted at the source location is unknown.
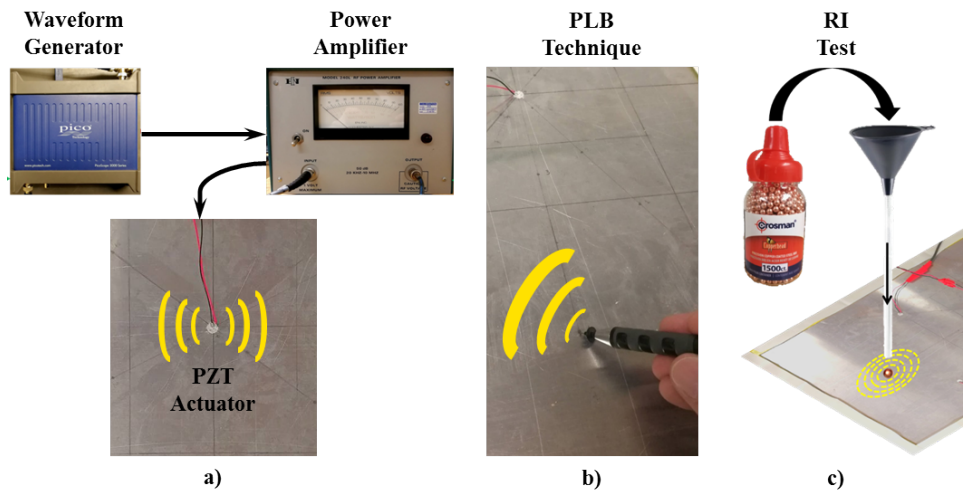

Figure 2: a) Experimental set-up to emit a signal from a surface bonded PZT actuator; b) The PLB technique; c) The RI test

2.2. Signal Reception

The received signal was measured through PZT sensors connected to an AEPH5 Pre-Amplifier with a gain set to 36 dB. The amplified electrical signal was gathered by the AMSY-6 AE-measurement system from Vallen AE-Measurement Système. This system collects the data with a sampling frequency of 5 MHz. The sampled data can be successively displayed on a monitor through its own DAQ software.

2.3. Plates

The first experimental setup consisted of a 7075-T651 aluminum plate measuring 304.8x609.6 mm^2 with a thickness of 1.6 mm. The dispersion curves of this aluminum plate were such that the fundamental S_0 and A_0 modes propagated below 1 MHz whereas the high order modes propagated at frequencies higher than 1 MHz. The second experimental setup consisted of an A572 low carbon steel plate measuring 609.6x609.6 mm^2 with a thickness of 13 mm. The dispersion curves of this steel plate were such that the fundamental S_0 and A_0 modes propagated below 150 kHz whereas the high order modes propagated at frequencies higher than 150 kHz. In particular, the S_1 mode is the fastest mode at 350 kHz. The two plates were setup with vacuum bag sealing tape on the plate edges, in order to decrease wave reflections at the plate boundaries.

2.4. Sensor Networks

A PZT transducer network of one PZT actuator and one PZT sensor were set on both plates in order to avoid attenuation complexities during the signal reconstruction process. The aluminum plate was setup with two Piezokinetic Sensors labelled as PZT 1 and PZT 2 whereas two Acellent Sensors named PZT 3 and PZT 4 were surface bonded on the steel plate as shown in Figure 3. The positions of these sensors are reported in

Figure 3. In this study SN_1 represents the sensor network on the aluminum plate, whereas SN_2 denotes the sensor network for the steel plate.

SN_1 and SN_2 are two analogous configurations because the PZT transducers are placed on the midline at 10 cm of distance with respect to the central points of the two plates. These two configurations are represented in Figure 3.a and 3.b respectively.
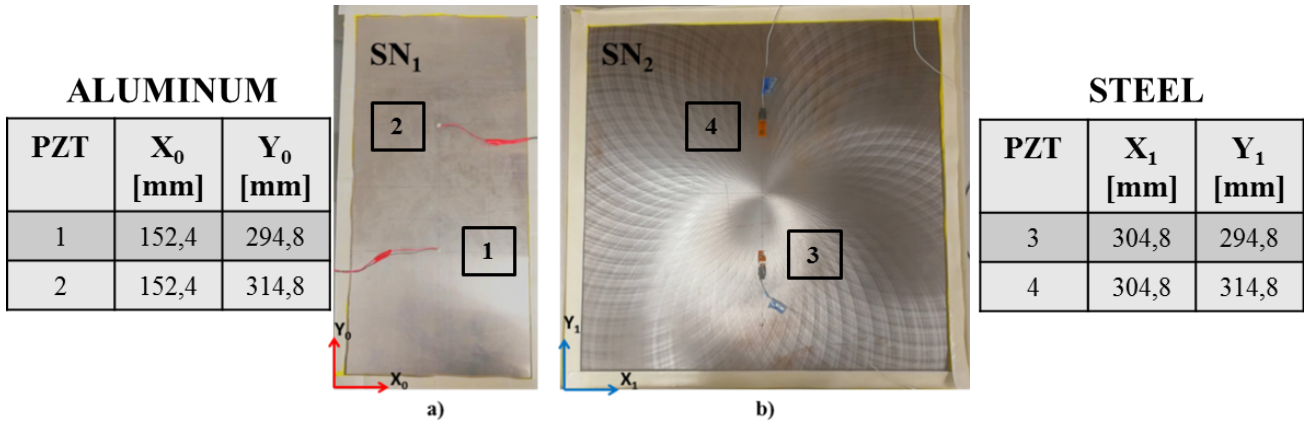

ALUMINUM		
PZT	X_0 **[mm]**	Y_0 **[mm]**
1	152,4	294,8
2	152,4	314,8

STEEL		
PZT	X_1 **[mm]**	Y_1 **[mm]**
3	304,8	294,8
4	304,8	314,8

Figure 3: a) SN_1 Configuration; b) SN_2 Configuration

2.5. Frequencies Compensation Transfer Function Creation Process

The FCTF derivation process is the same for both sensor network configurations. Figure 4 points out the FCTF creation process step by step for the configuration SN_1.
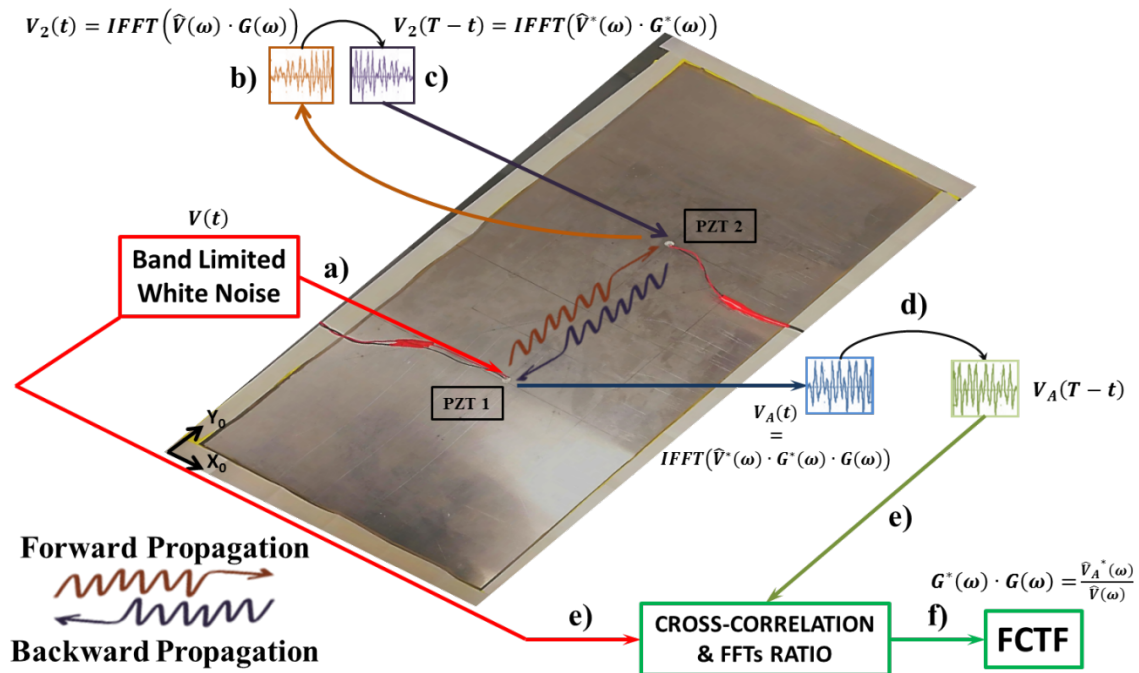

Figure 4: FCTF creation process

Referring to Figure 4, the following steps explain how the FCTF was developed:

a) A normalized Band Limited White Noise (BLWN) with frequencies up to 1 MHz was generated in Matlab[TM] and used as input signal to the system as shown in the set-up in Figure 2.a. The signal was filtered using a 6th-order Butterworth low-pass filter. The BLWN was characterized by a null mean and a standard deviation of 0.1. An amplified version of this input signal, with a maximum amplitude of 40 Volt, was sent from the PZT 1. We call this input signal $V(t)$.

b) As a consequence, PZT 2 received a distorted version of the input signal $V_2(t)$ such that $V_2(t) = IFFT\left(\hat{V}(\omega) \cdot G(\omega)\right)$. The symbol $IFFT$ represents the Inverse Fast Fourier Transform. Furthermore, $\hat{V}(\omega)$ and $G(\omega)$ represent the FFT of the input signal $V(t)$ and the frequency dependent transfer function for the forward propagation between the PZT 1 and PZT 2. The first wave packet of the received signal was isolated, re-sampled, normalized and time-reversed in Matlab™. The time reversed signal is represented by $V_2(T - t) = IFFT\left(\hat{V}^*(\omega) \cdot G^*(\omega)\right)$ where the symbol (*) represents the complex-coniugate.

c) The time-reversed signal was amplified up to 40 V and sent back. In this step the roles were interchanged, PZT 2 became the actuator and PZT 1 became the sensor.

d) PZT 1 received an output signal $V_A(t)$ which was a distorted version of the time-reversed signal such that $V_A(t) = IFFT\left(\hat{V}^*(\omega) \cdot G^*(\omega) \cdot G(\omega)\right)$. The first wave packet of the output signal was isolated, normalized and time-reversed. The time-reversed output was then $V_A(T - t)$.

e) A cross-correlation was performed between the BLWN input signal $V(t)$ and the time-reversed output signal $V_A(T - t)$ in order to align these two signals. Furthermore, the ratio between the FFT of these two signals was performed.

f) The FFT ratio of the previous step allowed to obtain a set of data point representative of the FCTF $G^*(\omega) \cdot G(\omega)$ since $G^*(\omega) \cdot G(\omega) = V_A^*(\omega)/\hat{V}(\omega)$.

Steps (a) through (f) were repeated ten times in order to obtain a cloud of data to interpolate, and thus a reliable trend of the FCTF. The previous steps and the formulas derivation are inspired from [20], with some differences due to the experimental approach adopted in this study.

2.6. Signal Reconstruction and Verification Process

The signal reconstruction process represents the last section of the methodology. Firstly, the first four sub-steps (a through d) of section 2.5 are repeated with another input signal $V(t)$. This time the input signal $V(t)$ is represented by one of the four signal sources introduced in section 2.1. If the signal source is a HW or a NBLB signal, the input signal is amplified up to 40 V, to be consistent with the FCTF creation process.

For the case of a known input source signal $V(t)$, such as the HW and the NBLB signals, once the time-reversed output signal $V_A(T - t)$ is obtained, a cross-correlation can be performed between the input signal $V(t)$ and the time-reversed output signal $V_A(T - t)$ to align the two signals. Then the FCTF is applied to the time-reversed output signal FFT $V_A^*(\omega)$ to obtain the reconstructed signal FFT $\hat{V}_R(\omega)$. Finally, the IFFT is applied to $\hat{V}_R(\omega)$ to retrieve the reconstructed signal $V_R(t)$. A comparison can be made between the input signal $V(t)$ and the reconstructed signal $V_R(t)$ to verify the effectiveness of the proposed method.

For the case of an unknown input source signal $V(t)$, such as the PLB and RI signals emitted on the SN_1 configuration, it is impossible to perform a cross-correlation or a comparison between the time-reversed output signal $V_A(T - t)$ and the input signal $V(t)$ since the input signal $V(t)$ is unknown. Therefore, the FCTF is simply applied to the time-reversed output signal FFT $V_A^*(\omega)$ to obtain a hypothetical reconstructed spectrum FFT $\hat{V}_R(\omega)$. Then, the IFFT is applied to $\hat{V}_R(\omega)$ to retrieve the hypothetical reconstructed signal $V_R(t)$. To verify if the hypothetical reconstructed signal $V_R(t)$ matches with the unknown input signal $V(t)$, the hypothetical reconstructed signal $V_R(t)$ was sent from the PZT 1, placed at the source location which works now as a PZT actuator amplifying the signal up to 40 Volt (i.e. the roles are interchanged a second time between the PZT actuator and the PZT sensor). A distorted version of the reconstructed signal $V_{2-R}(t)$ is received at the PZT 2. Finally, $V_{2-R}(t)$ was compared with $V_2(t)$ to verify the effectiveness of the method.

It is relevant to highlight that the HW and NBLB signals were reconstructed for both plates to prove the possibility to extend the FCTF method to different materials whereas the PLB and RI signals were reconstructed focusing on the aluminum plate.

3. Results

3.1. Aluminum and Steel Frequencies Compensation Transfer Functions

Thanks to the methodology presented in section 2.5, the aluminum FCTF $(G^*(\omega) \cdot G(\omega))_{ALU}$ and the steel FCTF $(G^*(\omega) \cdot G(\omega))_{STEEL}$ are derived with a smoothing spline interpolation up to 1 MHz. Both FCTFs are represented in Figure 5.a and Figure 5.b for the aluminum and steel plates respectively. The red dotted line separates two regions. When the FCTF is underneath the red dotted line the frequencies are attenuated whereas above the red dotted line, the frequencies are amplified.
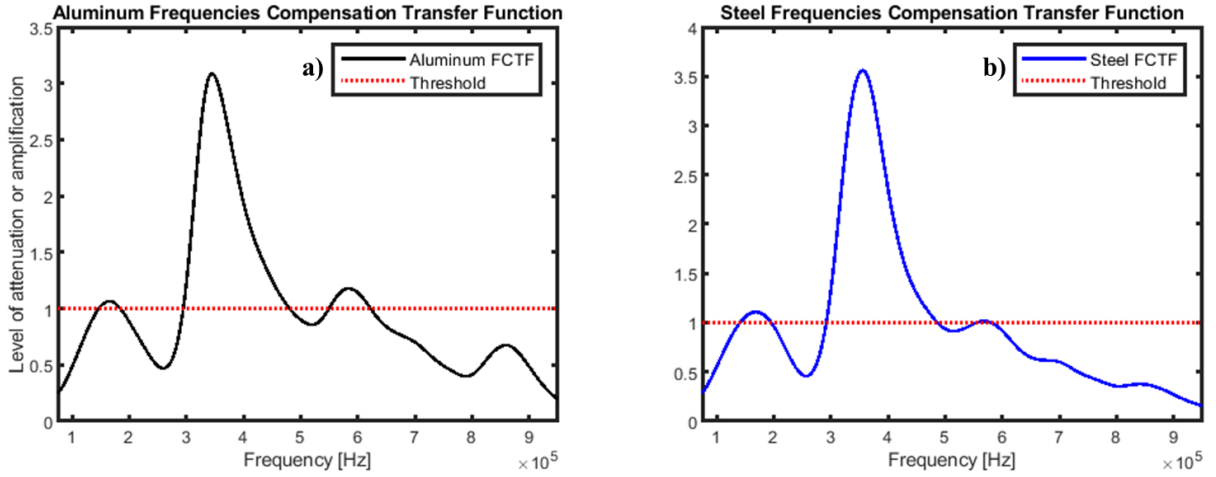

Figure 5: a) Aluminum FCTF; b) Steel FCTF

3.2. Hanning Window and Numerical Band Limited Broadband (NBLB) signals reconstruction on aluminum and steel plates

If the HW or the NBLB signals represent the input source signal $V(t)$, then applying the FCTF to the time-reversed output signal FFT $V_A^*(\omega)$, we can reconstruct the signal $V_R(t)$ and compare it with the input signal $V(t)$ as explained in section 2.6. As such, Figures 6.a to 6.d show the comparison between $V(t)$ and $V_A(T-t)$ and between $V(t)$ and $V_R(t)$ for both material cases when the HW at 350 kHz is used as input signal $V(t)$. For each case, Figure 6 introduces the maximum Normalized Cross-correlation Coefficient (NCC). The maximum NCC is theoretically equal to one when two signals are exactly the same.
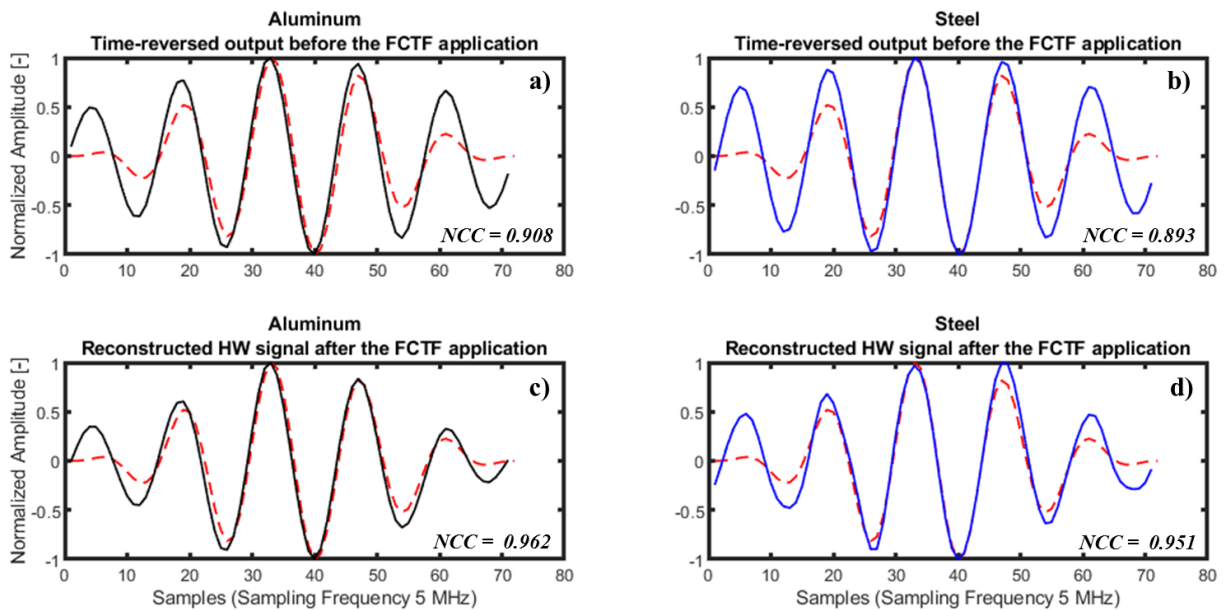

Figure 6 : Comparison between a) $V(t)$ (red dotted line) and $V_A(T-t)$ (black line) on aluminum; b) $V(t)$ and $V_A(T-t)$ (blue line) on steel; c) $V(t)$ and $V_R(t)$ (black line) on aluminum; d) $V(t)$ and $V_R(t)$ (blue line) on steel

On the other hand, Figures 7.a to 7.d show the comparison between $V(t)$ and $V_A(T - t)$ and between $V(t)$ and $V_R(t)$ for both material cases when the NBLB signal is used as input signal $V(t)$ for both the aluminum and steel plates. In both figures, the red dotted line represents the original signal while the solid line represents the reconstructed signal. The maximum NCC is reported for each case in Figure 7.
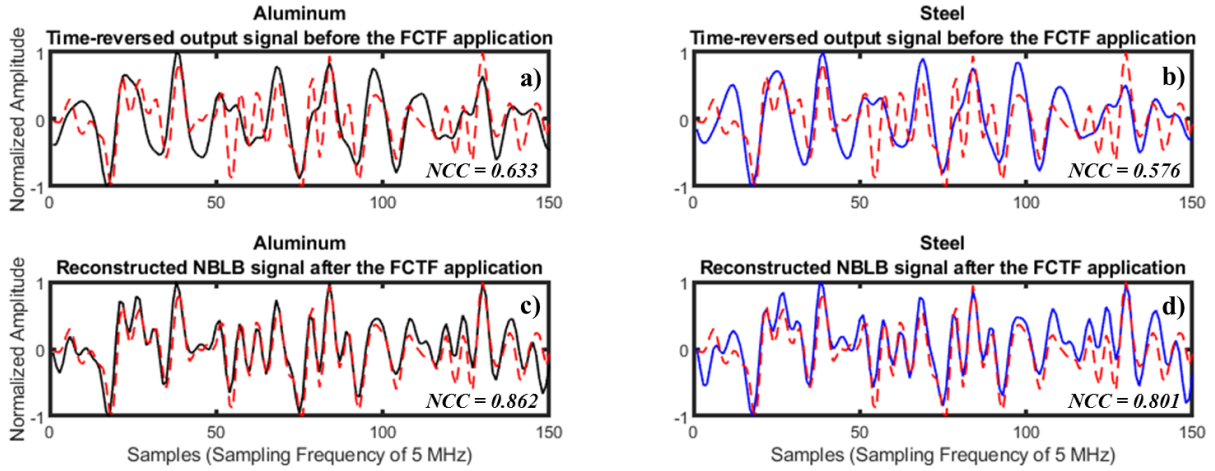

Figure 7 : Comparison between a) $V(t)$ (red dotted line) and $V_A(T - t)$ (black line) on aluminum; b) $V(t)$ and $V_A(T - t)$ (blue line) on steel; c) $V(t)$ and $V_R(t)$ (black line) on aluminum; d) $V(t)$ and $V_R(t)$ (blue line) on steel

3.3. Pencil Lead Break and Rock Impact signals reconstruction on aluminum plate

In this section, the PLB and RI signals are the unknown source input signals emitted in the SN_1 configuration. In Figures 8.a and 8.b are represented by the time-reversed output signal $V_A(T - t)$ and the hypothetical reconstructed signal $V_R(t)$ for the PLB and RI cases respectively on the aluminum plate. In this figure the magenta line represents $V_A(T - t)$ signal while the black line represents the reconstructed signal $V_R(t)$ after the application of the FCTF.
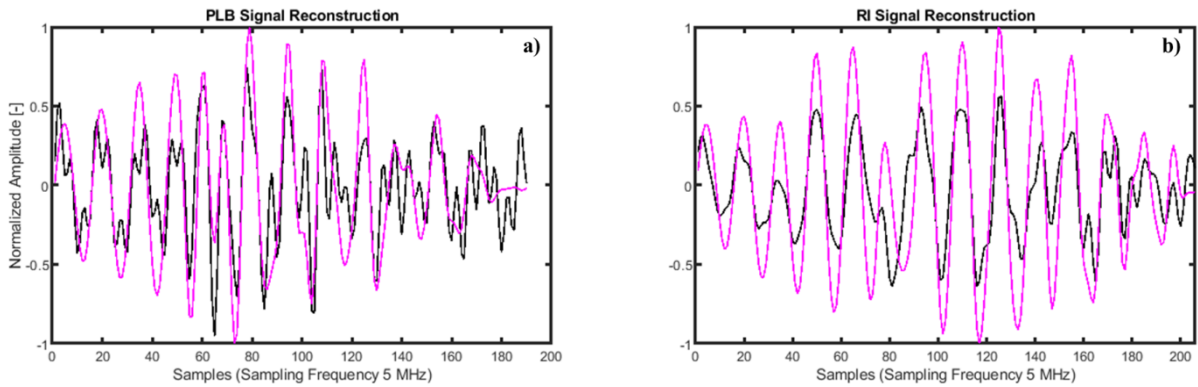

Figure 8: a) $V_A(T - t)$ before the FCTF application (magenta line) and $V_R(t)$ after the FCTF application (black line) on aluminum for the PLB case; b) $V_A(T - t)$ before the FCTF application (magenta line) and $V_R(t)$ after the FCTF application (black line) on aluminum for the RI case

Figures 9.a and 9.b shows the verification step introduced in section 2.6 where the signals $V_2(t)$ and $V_{2-R}(t)$ are compared after the normalization and cross-correlation of the S_0 wave packets for the PLB and RI cases respectively on the aluminum plate. The maximum NCC is introduced for both cases in Figures 9.a and 9.b respectively.
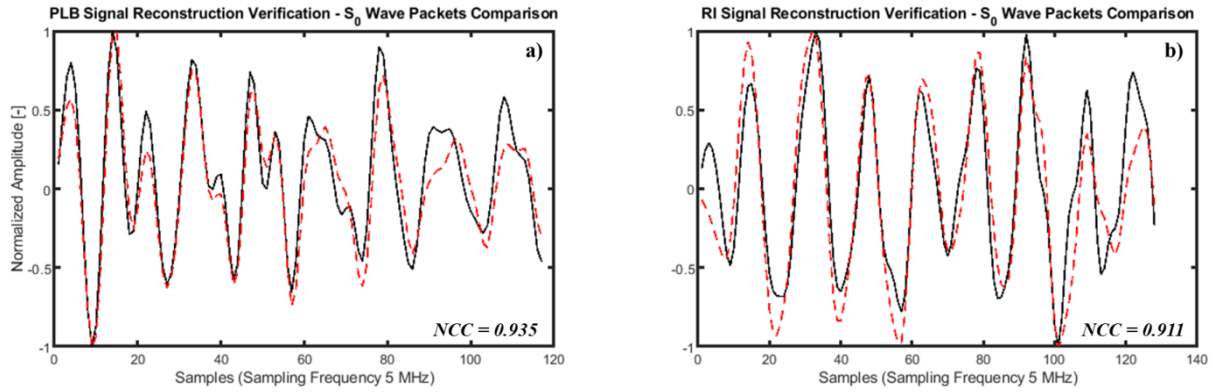
Figure 9: Comparison between the normalized S_0 wave packets of a) $V_2(t)$ (red dotted line) and $V_{2-R}(t)$ (black line) on aluminum for the PLB case; b) $V_2(t)$ (red dotted line) and $V_{2-R}(t)$ (black line) on aluminum for the RI case

4. Discussion

In the aluminum plate, the FCTFs were developed based on the TR process of the first arriving wave packet at the PZT sensors using a BLWN as input signal as indicated in section 2.5. Moreover, the excited frequencies of the BLWN input signal are concentrated below 1 MHz. According to this, the aluminum FCTF of Figure 5.a is built based on the TR process of the S_0 wave packet because the S_0 mode is the fastest mode below 1 MHz. However, for the steel plate the development of the FCTF is more complicated due to the presences of multiple S modes.

The derivation of the FCTF for the steel plate case is not trivial because below 1 MHz, several high order modes propagate at similar speeds in the steel plate such as S_0, S_1 and S_2 propagating in between 4700 and 4800 m/millisecond at approximately 100, 300 and 550 kHz respectively. As a consequence, it can be implied that the steel FCTF of Figure 5.b is based on the TR process of a wave packet composed by multiple modes propagating at similar speeds.

In comparing the FCTFs obtained based on the TR of the first wave packets captured by the PZT transducers for aluminum and steel, these FCTFs show a similar trend with a main amplification peak localized between 300 kHz and 400 kHz as shown in Figures 5.a and 5.b respectively. These similar trends seem to indicate that the FCTF is material independent. In addition, it is important to note that the dimensions of the plate like structure and the sensor type used in both experimental setups were different. Further studies and experiments must be conducted to fully understand the variables playing a role in the development of the FCTF. Regardless of the material, the application of the TR to a central frequency signal can be achieved in both aluminum and steel plates.

In the case of the aluminum plate, knowledge of the dispersion curves dictate that at 350 kHz the first arriving wave packet is the S_0 wave packet. This means that the HW signal of Figure 6.c is reconstructed based on the TR process of the S_0 wave packet which has been well documented in the literature. However, the application of the aluminum FCTF allows for an improvement of the HW reconstruction in terms of maximum NCC passing from the time-reversed output signal $V_A(T - t)$ in Figure 6.a to the reconstructed signal $V_R(t)$ in in Figures 6.c. A maximum NCC improvement of around 6% was observed. Such results seem to indicate that the FCTF method can be applied successfully to aid in the reconstruction of HW signals based on the TR process on an aluminum plate.

Analogously to the aluminum plate, from knowledge of the dispersion curves for steel plates, it was known that the first arriving wave packet at 350 kHz was the S_1 wave packet. This indicates that the HW signal of Figure 6.d is reconstructed based on the TR process of the S_1 wave packet for the steel. In addition, in this case the application of the steel FCTF allows for an improvement of the HW reconstruction in terms of maximum NCC passing from the time-reversed output signal $V_A(T - t)$ in Figure 6.b to the reconstructed signal $V_R(t)$ in Figure 6.d. A maximum NCC improvement of around 6% was observed. As a conclusion, the FCTF method can be applied successfully for the reconstruction of HW signals on a steel plate and can be based on the TR process of a single and high order mode wave packet such as the S_1 mode.

The comparison between the HW reconstructions on both plates shows some interesting similarities. Firstly, the reconstructions of the HW is improved thanks to the application of both FCTFs, in particular for the external parts of the HW comparing Figures 6.a and 6.b with the Figures 6.c and 6.d respectively. Secondly, an improvement in terms of maximum NCC before and after the FCTF application for both plates is observed. The difference between the maximum NCCs of Figure 6.c and 6.a in the aluminum case leads to a ΔNCC of 0.054 whereas the difference between the maximum NCCs of Figure 6.d and 6.b in the steel case leads to a ΔNCC of 0.058. Both ΔNCC for both material cases are quasi-equal. These results indicate that the improvement in terms of maximum NCC before and after the application of both FCTFs for the reconstruction of the HW is practically the same, both around 6%. This last conclusion can be attributed to the similarity between both FCTFs. Indeed, due to the similarity between the two FCTFs, we can expect to obtain a comparable error reduction on the signal reconstruction after the application of both FCTFs.

In contrast to the HW signal which is known to have a central frequency, the NBLB signal contains frequency peaks until 1 MHz which means that both the S_0 wave packet and the A_0 wave packet propagated on the aluminum plate. However, the reconstruction of the NBLB signal in the aluminum plate is based only on the S_0 wave packet which is the fastest mode. Moreover, the application of the aluminum FCTF allowed for an improvement of the NBLB signal reconstruction in terms of maximum NCC passing from the time-reversed output signal $V_A(T - t)$ in Figure 7.a to the reconstructed signal $V_R(t)$ in Figure 7.c, with an NCC improvement of 36%. Similarly to the conclusions brought for the HW reconstruction, this result confirms that the reconstruction of a NBLB signal through the FCTF method can be performed based on the TR process of a single wave packet.

However, for the NBLB signal reconstruction on the steel plate, other considerations were made. Indeed, since the NBLB signal contains frequency peaks up to 1 MHz, the propagation of different wave packets with similar speeds occurs in the steel plate, such as for example the S_0, S_1 and S_2 propagating in between 4700 and 4800 m/millisecond at approximatively 100, 300 and 550 kHz respectively. This indicates that the first arriving wave packet at the PZT transducer is of difficult interpretation and could be a combination of several high order modes travelling at a similar speed. Nevertheless, the reconstruction is still viable also in this case, since the trend of the original signal is kept after the application of the FCTF with an improvement of approximatively 39% on the maximum NCC shown in Figure 7.d. It is possible to associate this reconstruction improvement in the steel plate with the creation process of the steel FCTF. As previously stated, the steel FCTF is also built thanks to the TR process of a multi-mode wave packet signal. Thus, both the reconstruction of the NBLB signal and the creation process of the steel FCTF are based on the TR process of multi-mode wave packets propagating below 1 MHz. Since both signals are based on a similar and consistent TR process, as a consequence an efficient reconstruction is obtained for the NBLB signal in the steel plate after the application of the steel FCTF to the time-reversed output signal $V_A(T - t)$.

When comparing the NBLB reconstruction for both plates following the same procedure for the comparison of the HW reconstructions, the two ΔNCC were calculated, these showed an improvement of the signal reconstruction. The ΔNCC obtained considering the maximum NCC difference between Figures 7.c and 7.a was 0.229 whereas the ΔNCC obtained considering the maximum NCC difference between Figures 7.d and 7.b was 0.225. Since these results are quasi-equal, they support the conclusion already mentioned that the same error reduction is observed on the signal reconstructions after the application of the FCTFs of both materials, because both FCTFs are similar.

However, in all previous cases the authors knew what the outcome should be, as the signals being reconstructed, whether broadband in nature or signals of a central frequency were engineered by the authors to test the methodology. Nevertheless, the authors were curious to understand what would happen if an attempt was made to reconstruct an unknown signal such as PLB or RI. As such, the verification process for the reconstruction of real BdB signals such as the PLB and RI signals on aluminum plate was conducted. It is important to note that the results for these two signals (PLB and RI) were performed only for the S_0 wave packets of the $V_2(t)$ and $V_{2-R}(t)$ signals. Since the authors did not have the original signal, the reconstructed signals represented in Figures 8.a and 8.b were sent from the same location using the same PZT actuator used to capture the output signal $V_A(t)$. Only the S_0 wave packet was used during the verification process in order to avoid the effect of the reflections from the border of the plate. The verification consisted in comparing the reconstructed signal once this was sent to the sensor with the original

PLB and/or RI. This resulted in a high value of the maximum NCC (over 90%) as shown in Figures 9.a and 9.b. These results suggest that the FCTF method applied to a real BdB signal allows for the reconstruction of a single wave packet.

5. Conclusion

In this study, an innovative experimental TR process based on the creation and application of a FCTF has been used for the reconstruction of different signal sources on different types of materials. The input signal consisted on HW and NBLB signals designed on Matlab^{TM} and unknown PLB and RI signals. In particular, it was demonstrated the effectiveness of this method for the improvement of the reconstruction of simple NwB signals such as HW and more complex signals such as NBLB signals in terms of maximum Normalized Cross-correlation Coefficient (NCC) opening the perspective for the reconstruction of complex signals on different materials other than aluminum. The results showed that such improvement on the reconstruction of the HW and the NBLB was similar for both materials (NCC increment of around 6% for the HW, and around 37% for the NBLB signal reconstruction), suggesting that the method is independent on the material type, plate dimensions and the sensor type. Finally, the FCTF method has been applied for the reconstruction of unknown signal sources such as PLB signal source or a RI signal source. In this last application, the method was shown to be effective for the frequency compensation of a single wave packet (S_0), effectiveness quantified by the comparison of the response signal collected from the propagation of the actual PLB and RI, and the ones obtained as their hypothetical reconstructions. The maximum NCC for these comparisons was 0.935 and 0.911 for PLB and RI respectively. These first results open the possibility for the reconstruction of complex real BdB signal. Indeed, since the FCTF methods work for a single wave packet such as S_0 in the aluminum case for the reconstruction of real BdB signals, it can be thought that through the creation of a second FCTF based on the A_0 wave packet, it will be possible to reconstruct entirely a real BdB signal for both modes.

Bibliography

[1]   Charles R. Farrar, Keith Worden, "An introduction to structural health monitoring", *Philosophical Transactions of the Royal Society A Mathematical Physical and Engineering Sciences,* vol. 365, no. 1851, p. 303–315, 2007.
[2]   Daniel Balageas, Claus-Peter Fritzen, Alfredo Güemes, Structural Health Monitoring, ISTE, 2006.
[3]   T.M. Roberts, M. Talebzadeh, " Acoustic Emission Monitoring of Fatigue Crack Propagation ", *Journal of Constructional Steel Research*, vol.59, 2003.
[4]   S. Benmedakhene, M. Kenane, M. L. Benzeggagh, " Initiation and growth of delamination in glass/epoxy composites subjected to static and dynamic loading by acoustic emission monitoring ", *Composites Science and Technology*, vol.59, 1999.
[5]   K. Diamanti, J. M. Hodgkinson, C. Soutis, " Detection of Low-velocity Impact Damage in Composite Plates using Lamb Waves ", *Structural Health Monitoring*, vol.3, 2004.
[6]   H. L. Dunegan, D. O. Harris, C.A. Tatro, " Fracture Analysis by use of Acoustic Emission ", *Engineering Fracture Mechanics*, vol.1, 1968.
[7]   S. Wagle, H.Kato, " Ultrasonic detection of fretting fatigue damage at bolt joints of aluminum alloy plates ", *International Journal of Fatigue*, vol.31, 2009.
[8]   M. Adler, M. de Billy, G. Quentin , " Evaluation of friction-welded aluminum-steel bonds using dispersive guided modes of a layered substrate ", *Journal of Applied Physics*, vol.68, 1990.
[9]   H. Lamb, "On Waves in an Elastic Plate", *Proceedings of the Royal Society,* vol. 93, no. 648, 1917.
[10]   J.Von Hann, Handbook of Climatology, Macmillan, 1903.
[11]   Markus G.R. Sause, '' Investigation of Pencil-Lead Breaks as Acoustic Emission Sources '', *Journal AE*, vol.29, July 2013.
[12]   Mathias Fink, "Time Reversal of Ultrasonic Fields – Part I : Basic Principles ", *IEEE Transactions on Ultrasonics, Ferroelectrics and Frequency Control,* vol. 39, no.5, September 1992.
[13]   Mathias Fink, '' Time Reversed Acoustics '', *Physics Today*, vol.50, no.3, 1997.
[14]   R.K. Ing, M. Fink, "Time-Reversed Lamb Waves," *IEEE Transactions on Ultrasonics, Ferroelectrics and Frequency Control,* vol. 45, pp. 1032-1043, 1998.

[15] CH Wang, JT Rose, FK Chang,, "A Computerized Time-reversal Method for Structural Health Monitoring," in Proceedings of SPIE Conference on Smart Structures and NDE, San Diego, CA, USA, 2003.

[16] JT Rose, CH Wang, "Mindlin plate theory for damage detection I, source solutions,", *J. Acoust. Soc. Am.*, vol. 116, no. 1, p. 154–171, 2004.

[17] Buli Xu, Victor Giurgiutiu, '' Single Mode Tuning Effects on Lamb Wave Time Reversal with Piezoelectric Wafer Active Sensors for Structural Health Monitoring '', *Journal of Nondestructive Evaluation*, Springer, 2007.

[18] V.Giurgiutiu, "Tuned Lamb-wave excitation and detection with piezoelectric wafer active sensors for structural health monitoring.", *J. Intelligent Material Systems and Structures*, **16**(4), 291–306, 2005.

[19] Hyun Woo Park, Seung Bum Kim, Hoon Sohn, '' Understanding a time reversal process in Lamb wave propagation '', *Wave Motion*, vol.46, Elsevier, 2009.

[20] F.Falcetelli, M.B.Romero, E.Troiani, M.Martinez, "Modelling of a Pencil Lead Break Acoustic Emission Sources using the Time Reversal Technique", 9th European Workshop on Structural Health Monitoring, July 10-13, 2018, Manchester, United Kingdom.

[21] J.Wang, Y.Shen, "An enhanced Lamb wave virtual time reversal technique for damage detection with transducer transfer function compensation ", *Smart Materials and Structures*, vol.28, no.8, July 2019.

[22] ASTM E-976, Standard Guide for Determining the Reproducibility of Acoustic Emission Sensor Response, ASTM International